

RESEARCH ARTICLE | OCTOBER 02 2024

## Hydrodynamic modulation instability triggered by a two-wave system

Special Collection: [Rogue waves: Theory, Methods and Applications](#)

Yuchen He ; Jinghua Wang ; Bertrand Kibler ; Amin Chabchoub  



Chaos 34, 103108 (2024)

<https://doi.org/10.1063/5.0220359>



View  
Online



Export  
Citation

### Articles You May Be Interested In

Periodic orbits in Fermi–Pasta–Ulam–Tsingou systems


*Chaos* (September 2024)

Four-wave mixing and coherently coupled Schrödinger equations: Cascading processes and Fermi–Pasta–Ulam–Tsingou recurrence

*Chaos* (August 2021)

Recurrence recovery in heterogeneous Fermi–Pasta–Ulam–Tsingou systems


*Chaos* (September 2023)



Chaos

## Special Topics Open for Submissions

[Learn More](#)



AIP  
Publishing

# Hydrodynamic modulation instability triggered by a two-wave system

Cite as: Chaos 34, 103108 (2024); doi: 10.1063/5.0220359

Submitted: 24 May 2024 · Accepted: 3 September 2024 ·

Published Online: 2 October 2024



View Online



Export Citation



CrossMark

Yuchen He,<sup>1,2,a)</sup> Jinghua Wang,<sup>1,3,4)</sup> Bertrand Kibler,<sup>5)</sup> and Amin Chabchoub<sup>6,7,8,b)</sup>

## AFFILIATIONS

<sup>1</sup>Department of Civil and Environmental Engineering, The Hong Kong Polytechnic University, Hong Kong 999077, China

<sup>2</sup>Department of Ocean Science and Engineering, Southern University of Science and Technology, Shenzhen 518055, China

<sup>3</sup>Research Institute for Sustainable Urban Development, The Hong Kong Polytechnic University, Hong Kong 999077, China

<sup>4</sup>Shenzhen Research Institute, The Hong Kong Polytechnic University, Shenzhen 518057, China

<sup>5</sup>Laboratoire Interdisciplinaire Carnot de Bourgogne, UMR6303 CNRS-UBFC, 21000 Dijon, France

<sup>6</sup>Disaster Prevention Research Institute, Kyoto University, Uji, Kyoto 611-0011, Japan

<sup>7</sup>Marine Physics and Engineering Unit, Okinawa Institute of Science and Technology, Onna-son, Okinawa 904-0495, Japan

<sup>8</sup>Department of Infrastructure Engineering, The University of Melbourne, Parkville, Victoria 3010, Australia

**Note:** This paper is part of the Focus Issue, Rogue waves: Theory, Methods and Applications.

**a) Electronic mail:** [yuchen.he@polyu.edu.hk](mailto:yuchen.he@polyu.edu.hk)

**b) Author to whom correspondence should be addressed:** [amin.chabchoub@oist.jp](mailto:amin.chabchoub@oist.jp)

## ABSTRACT

The modulation instability (MI) is responsible for the disintegration of a regular nonlinear wave train and can lead to strong localizations in the form of rogue waves. This mechanism has been studied in a variety of nonlinear dispersive media, such as hydrodynamics, optics, plasma, mechanical systems, electric transmission lines, and Bose–Einstein condensates, while its impact on applied sciences is steadily growing. It is well-known that the classical MI dynamics can be triggered when a pair of small-amplitude sidebands are excited within a particular frequency range around the main peak frequency. That is, a three-wave system, consisting of the carrier wave together with a pair of unstable sidebands, is usually adopted to initiate the wave focusing process in a numerical or laboratory experiment. Breather solutions of the nonlinear Schrödinger equation (NLSE) revealed that MI can generate much more complex localized structures, beyond the three-wave system initialization approach or by means of a continuous spectrum. In this work, we report an experimental study for deep-water surface gravity waves asserting that a MI process can be triggered by a single unstable sideband only, and thus, initialized from a two-wave process when including the contribution of the peak frequency. The experimental data are validated against fully nonlinear hydrodynamic numerical wave tank simulations and show very good agreement. The long-term evolution of such unstable wave trains shows a distinct shift in the recurrent Fermi–Pasta–Ulam–Tsingou focusing cycles, which are captured by the NLSE and fully nonlinear hydrodynamic simulations with some distinctions.

Published under an exclusive license by AIP Publishing. <https://doi.org/10.1063/5.0220359>

Localized wave patterns in nonlinear dispersive media can occur as a result of modulation instability, which is triggered by small perturbations of frequency and amplitude. The following energy transfer from carrier wave to the sidebands ensures the broadening of the wave spectrum and focusing of the wave field in physical space. This is also known as the Benjamin–Feir instability of quasi-four-wave resonant interactions in the context of surface gravity ocean waves. In fact, Benjamin and Feir applied

the linear stability analysis to a Stokes wave being perturbed by a symmetric sideband pair to determine the range of unstable modulation frequencies. We provide experimental evidence for water waves that this fundamental instability can also be precipitated by a single sideband seeding. Despite the formation of the opposite sidebands at a later stage, due to the symmetric energy transmission from the carrier to the sidebands, the long-term evolution of the unstable wave field reveals shifted focusing recurrence cycles.

## I. INTRODUCTION

Waves in nonlinear dispersive media can become unstable when subjected to long-wave perturbations.<sup>1–4</sup> Such an intriguing transfer of energy process from the peak frequency to sidebands is known as modulation instability (MI) and is not unique to water waves, for which it was first experimentally observed.<sup>5–8</sup> The result of the linear stability analysis of second-order Stokes waves provides an exact range of unstable frequencies in which a pair of small-amplitude sidebands around the peak frequency will start to grow exponentially resulting in a disintegration and periodic wave group focusing of the wave field.<sup>9</sup> The same result can be obtained if applying the linear stability analysis to the regular envelope solution of the nonlinear Schrödinger equation (NLSE).<sup>3,10</sup> Despite its numerous physical limitations, investigating the MI using the NLSE at that order of approximation in wave steepness is more diligent since the framework can reasonably predict the saturation of sidebands' growth, their decay, and the follow-up Fermi–Pasta–Ulam–Tsingou (FPUT) focusing recurrence.<sup>10–19</sup> Moreover, exact solutions, such as the famed Akhmediev (ABs) and Peregrine breathers,<sup>20,21</sup> describe the nonlinear stage of modulation instability and are useful to trigger and control the dynamics of modulationally unstable waves in laboratory environments at any stage of evolution.<sup>22–28</sup> Note that doubly periodic A-type ABs can also describe the MI even outside the conventional MI instability band.<sup>29–31</sup>

Here, we report results of an experimental campaign aiming at the investigation of the initialization of MI for surface gravity waves from a two-wave system, i.e., a carrier frequency and only one small-amplitude sideband inclusion instead of exciting a pair of two, as suggested from the linear stability analysis. To initiate the evolution either in our numerical or physical wave tank, we use both, a spectrally truncated AB formalism, which consists of removing all higher or lower frequencies with the respect to the peak frequency, and a single-seeded sideband to a regular water wave train. Similarly to previous experiments in optics,<sup>23,32</sup> we confirm that one sideband is sufficient to trigger the instability dynamics in hydrodynamics, through an energy transfer from the carrier wave to the lower and higher sidebands, despite a slight delay in the focusing dynamics compared to the classical three-wave excitation. The experiments are in very good agreement with the fully nonlinear numerical wave tank simulations. We also investigate the long-term behavior of unstable wave groups and show that these undergo a phase-shifted FPUT focusing recurrence<sup>17,33</sup> compared to the classical and non-shifted MI dynamics.

## II. FORMALISM

In their pioneering work, Benjamin and Feir showed that a second-order Stokes wave of amplitude  $a$ , wave frequency  $\omega = 2\pi f$ , and wavenumber  $k = \frac{2\pi}{\lambda}$

$$\eta_S(x, t) = a \cos[kx - \omega t] + \frac{1}{2}ka^2 \cos[2(kx - \omega t)] \quad (1)$$

is unstable to long-wave perturbation in the temporal domain, if the sidebands are triggered within the bounded modulation frequency range of<sup>9,34</sup>

$$0 < \Omega < \sqrt{2}ka\omega. \quad (2)$$

Intriguingly, the same condition can be found when applying the linear stability analysis on the constant and steady background envelope Stokes solution  $\psi_S(x, t) = a \exp(ia^2k^3x)$  of the time-like NLSE,<sup>3,10</sup>

$$i \left( \frac{\partial \psi}{\partial x} + \frac{1}{c_g} \frac{\partial \psi}{\partial t} \right) - \frac{k}{\omega^2} \frac{\partial^2 \psi}{\partial t^2} - k^3 |\psi|^2 \psi = 0. \quad (3)$$

Taking advantage of the integrability of the NLSE (3),<sup>35–37</sup> classes of exact solutions can describe the MI process beyond the non-physical predictions of the linear stability analysis, which for instance does not imply any saturation of the exponentially growing sidebands. In fact, the well-known ABs, parametrized as<sup>20,22</sup>

$$\psi_{AB}(x, t) = a \left( 1 + \frac{2(1 - 2a) \cosh(a^2k^3bx) + ib \sinh(a^2k^3bx)}{\sqrt{2a} \cos\left(\frac{ak}{\sqrt{2\omega}} \Omega\left(t - \frac{x}{c_g}\right)\right) - \cosh(a^2k^3bx)} \right) \times \exp(ia^2k^3x) \quad (4)$$

where  $b = \sqrt{8a(1 - 2a)}$  and  $a$  is the growth rate control parameter, accurately describe the complete MI focusing process, involving an infinite number of sidebands,<sup>20,38</sup> and an FPUT recurrence when linear dissipation is at play.<sup>17</sup> Over decades, numerical and laboratory experiments studying this classical universal instability have brought new insights and widened the application prospects to an old problem.<sup>17,26,39–48</sup> To ensure a rapid growth in the numerical and physical tank, we chose  $a = 0.25$ , which corresponds to the case of maximal growth rate.<sup>22</sup> In hydrodynamics and up to now, the initial or boundary conditions employed to initiate the instability dynamics were steadily symmetric, i.e., a pair of small-amplitude sidebands were employed to destabilize the regular or quasi-regular wave field. That said, experiments in optics<sup>23,32</sup> suggested and confirmed that MI can be also triggered from a single sideband only, i.e., from asymmetrical conditions. We will adopt this approach in this work to numerically and experimentally trigger the MI for surface gravity waves in an asymmetric manner, using AB-type and Stokes waves, and analyze the subsequent development of the unsteady wave trains.

## III. EXPERIMENTAL AND NUMERICAL PRELIMINARIES

The experiments have been conducted in a state-of-the-art wave flume with the dimensions of  $30 \times 1 \times 1 \text{ m}^3$ . Details regarding the apparatus and wave gauges used to ensure high resolution along the wave propagating direction can be found in Ref. 49. The perturbed Stokes wave analyzed has the amplitude  $a = 0.011 \text{ m}$ , wave frequency  $\omega = 3\pi \text{ s}^{-1}$ , and consequently a wavenumber of  $k = 9.08 \text{ m}^{-1}$  for the water depth of  $0.7 \text{ m}$ . The boundary conditions to generate modulationally unstable waves are determined either following the surface elevation profile of an exact AB to first-order in steepness, evaluated at  $x^* = -15 \text{ m}$  and defined as

$$\eta_{AB}(x^*, t) = \text{Re}(\psi_{AB}(x^*, t) \exp[i(kx^* - \omega t)]), \quad (5)$$

which is sufficient to accurately generate the periodic unstable wave packets, since Stokes wave shape is created, naturally including the mean flow component, even when the paddle's signal is strictly monochromatic. Note that our physical wave maker is equipped with a force feedback drive system, which controls paddle position,

velocity, and acceleration, and minimizes the generation of spurious waves according to Refs. 50 and 51. The same applies to the numerical wave maker. In order to investigate the frequency-asymmetric AB surface evolution, we apply a high- and a low-pass frequency filter to exclude all frequencies higher or lower than the peak frequency, which is at  $f = 1.5$  Hz, respectively. The alternative classical experimental approach to generate a monochromatic wave train, which is perturbed by a symmetric pair of sidebands, by a waver maker is parametrized as the following:

$$\eta_P(t) = a \cos[-\omega t] + \epsilon_R(t) + \epsilon_L(t), \quad (6)$$

where  $\epsilon_R(t) = \tilde{a}_R \cos[-\omega(1+\delta)t]$  and  $\epsilon_L(t) = \tilde{a}_L \cos[-\omega(1-\delta)t]$ . Note that the wave parameters at the initialization of wave dynamics  $\tilde{a}_R = \tilde{a}_L = 0.2a$  and  $\delta = \delta_{\max} = ak = 0.1$  have been chosen to meet the AB surface elevation model, as defined by Eq. (5), and satisfying the maximal instability growth rate condition. A single sideband perturbation can be trivially *switched off* by setting  $\tilde{a}_R = 0$  or  $\tilde{a}_L = 0$  in either  $\epsilon_R(t)$  or  $\epsilon_L(t)$ , respectively.

Part of the simulations considering long-term evolution dynamics advance the time-like NLSE (3) in space using the fourth-order Runge-Kutta and pseudospectral methods,<sup>52,53</sup> ensuring a high numerical accuracy. The spatial step length is  $dx = 0.0125$  m and the temporal resolution is  $dt = 0.2$  s, which are selected to also maintain stability of the simulations. To mitigate periodic boundary effects, the simulation domain size is set to 300 s, but only the central 60 s of data are extracted for spectral analysis and plotting purposes. Numerical dependence tests confirm that the chosen numerical steps, resolution, and domain size yield to high-fidelity results for the NLSE integration. The extraction of the wave envelope is achieved after the application of the Hilbert transform to the high- or low-pass frequency filtered AB surface elevation or perturbed Stokes waves, which are both described above. Note that the accuracy of the NLSE simulations have been validated through step dependence tests, and the selected spatial and time steps are both within the numerical stability range.

We also employ fully nonlinear hydrodynamic simulations for validation purposes. In order to capture the most accurate dynamics of the MI, these simulations were conducted based on the enhanced spectral boundary integral (ESBI) method. The ESBI framework accounts for high-order nonlinear effects and provides an accurate representation of nonlinear wave interactions. The numerical method used for these simulations is detailed and validated in the previous work.<sup>54</sup> Adopting the highest seventh order of convolution within the current study is particularly suited for simulating complex wave interactions.<sup>54–56</sup> Indeed, such a fully nonlinear framework provides a robust tool for understanding the formation and evolution of extreme wave events. The injection of the boundary condition (6) is achieved through an optimized pneumatic wave maker,<sup>57</sup> which introduces a prescribed varying pressure field at the water surface. Several iterations on the pressure field correction are adopted to ensure the wave generation accuracy, similarly to the physical wave maker.

#### IV. RESULTS AND VALIDATION

In this section, we report and discuss the results of the laboratory experiments performed starting from a standard AB at its early stage of evolution and followed by the cases of high- or low-pass frequency filtering with respect to the peak frequency. After that, we proceed with the corresponding analogous case by considering the classical double and then single-sideband perturbation of a second-order Stokes wave.

Figure 1 shows the results of wave envelope and spectral evolution for the Akhmediev breather case. We recall that the wave envelope is extracted from the water surface elevation by means of the Hilbert transform. We also align all measurements by the value of the deep-water group velocity value  $c_g = \frac{\partial \omega}{\partial k}$ . The beating of the AB wave field is clearly visible while the maximal compression occurs around 15 m from the wave maker, as suggested from

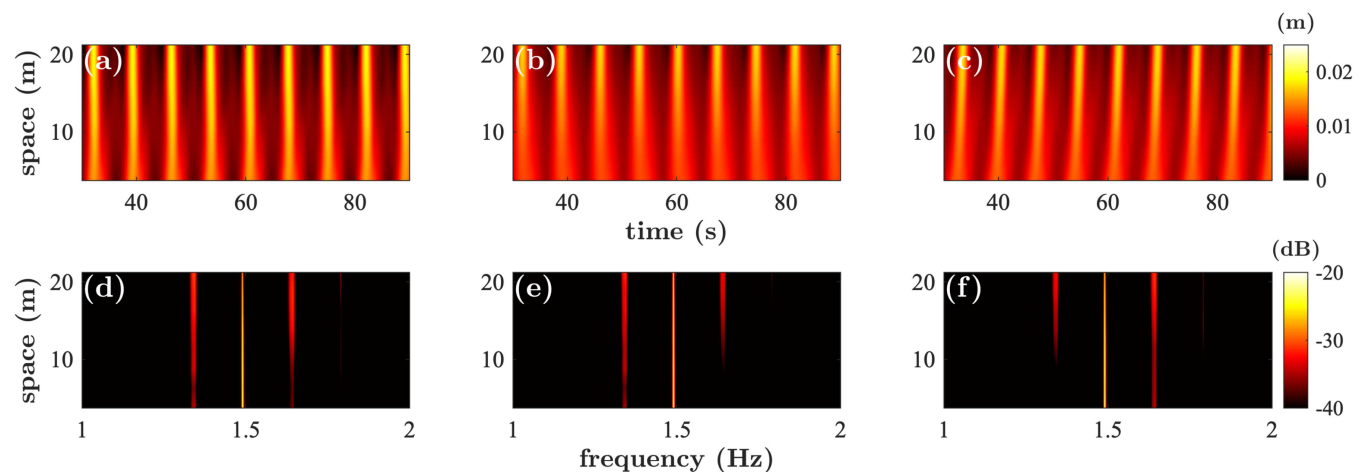


**FIG. 1.** Experimental wave evolution of (a) AB solution, (b) AB envelope including left sideband(s) only, and (c) AB envelope including right sideband(s) only. (d)–(f) Corresponding power spectra of wave elevation data from (a)–(c), respectively.

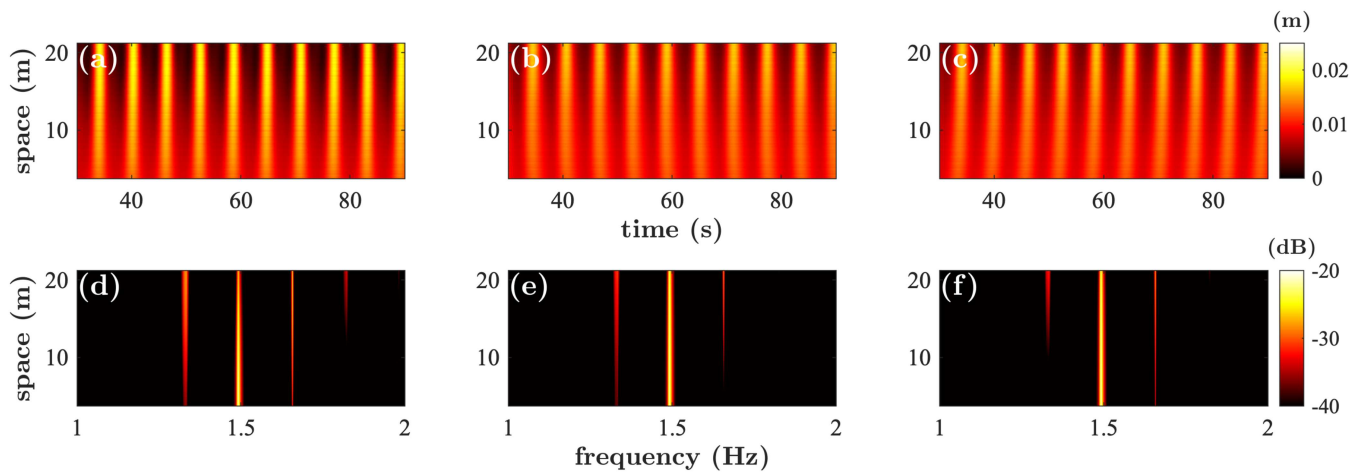


FIG. 2. Fully nonlinear numerical wave tank ESBI simulations corresponding to all respective cases in Fig. 1.

theory. Note that deviations of breather experiments with respect to NLSE theory has been discussed in Refs. 58 and 59.

Interestingly, a focusing of the wave field can be also observed when initiating the AB dynamics with the same boundary conditions, however, ignoring either the higher [Fig. 1(b)] or the lower [Fig. 1(c)] frequencies with respect to the peak frequency, located at  $f = 1.5$  Hz, in the boundary conditions. The main difference is that both evolution cases of the unstable nonlinear wave fields are delayed compared to the pure AB dynamics. Note that the initial AB-type sideband cascade is not yet developed when defining the boundary conditions at  $x^* = -15$  m, and thus, the contribution of the higher sideband pairs is not substantial at that early stage of evolution and as injected to the wave maker, despite being present. Also worth mentioning is that the omitted opposite

sideband appears later during the wave propagation. Such a retardation process as a result of non-idealized breather boundary conditions for water waves has been already discussed in Refs. 60 and 61. The experimental results are validated against fully nonlinear numerical wave tank ESBI simulations and as depicted in Fig. 2.

Indeed, the ESBI-based numerical wave tank surface elevation simulations accurately capture the nonlinear dynamics of the AB envelope solution together with the other two variants, demonstrating good agreement with the experimental data. This can be also noticed in all wave fields' spectral dynamics.

Next, we perform analogical experiments, however, by considering a perturbed second-order Stokes wave, see (6). Figure 3 shows the results.

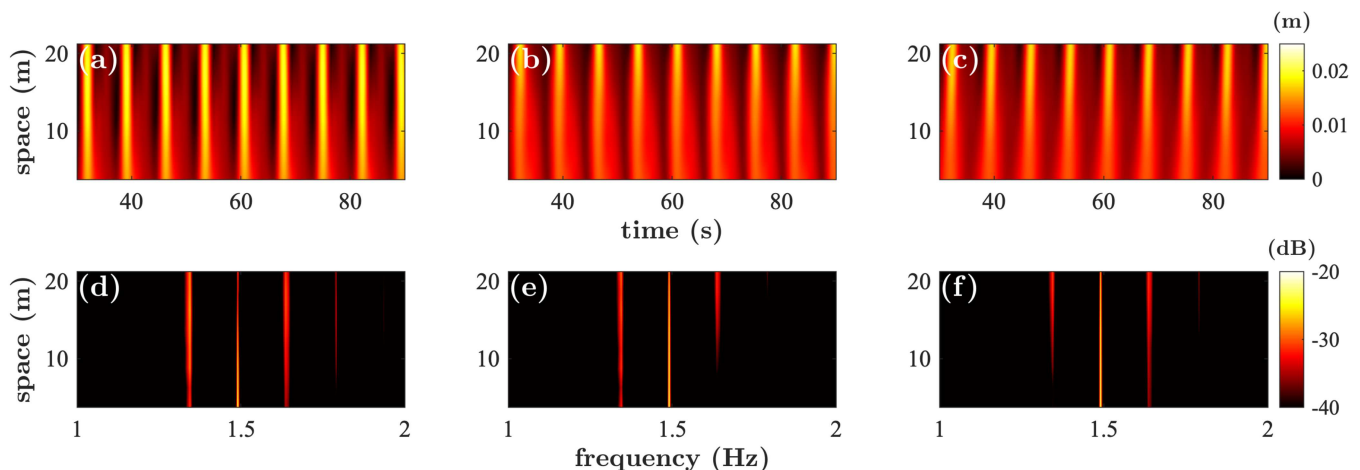


FIG. 3. Experimental wave envelope evolution of (a) Stokes wave perturbed with a symmetrical side-pair, (b) left sideband perturbation only, and (c) right sideband only. (d)–(f) correspond to the power spectra of wave elevation data from (a)–(c), respectively.



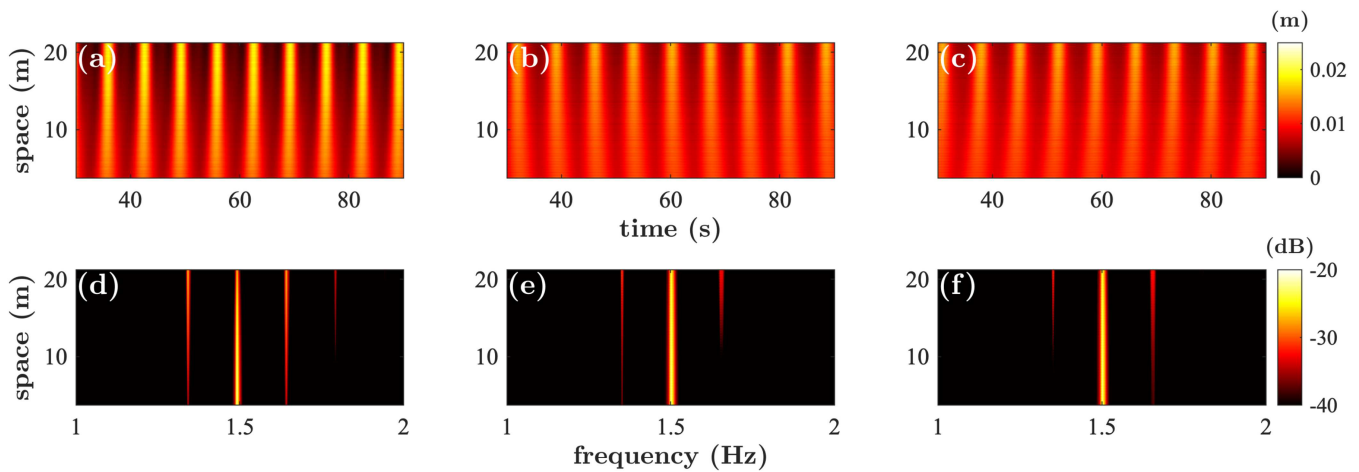


FIG. 4. Fully nonlinear ESBI simulations corresponding to Fig. 3.

Also in this case, we can distinctly observe the same wave focusing evolution trend, similarly to the AB case, which occurs when injecting one sideband perturbation only. This produces the same retardation of the focusing process as observed in the AB-type experiments. The same also applies to the ESBI simulations shown in Fig. 4.

This underlines not only the accuracy of our numerical wave tank simulations, but also and once again, the sufficiency of an

asymmetric one sideband only perturbation to trigger a MI-type nonlinear focusing of a quasi-regular wave field.

To compare the degree of accuracy of our numerical simulations to the collected wave data, as measured in the confined wave flume, Fig. 5 shows a comparison of the respective wave envelopes' maxima evolution for four cases, i.e., excitation of a pure AB, a symmetric perturbation a regular water wave train, a respective asymmetric sideband excitation (left then right).

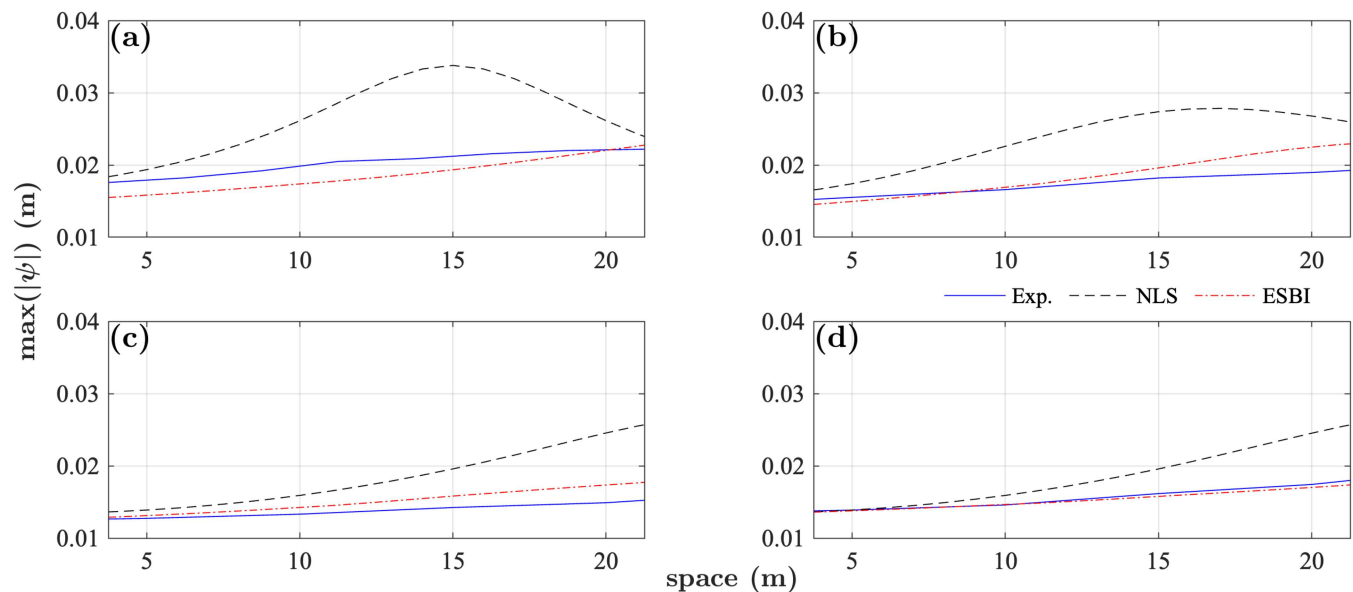
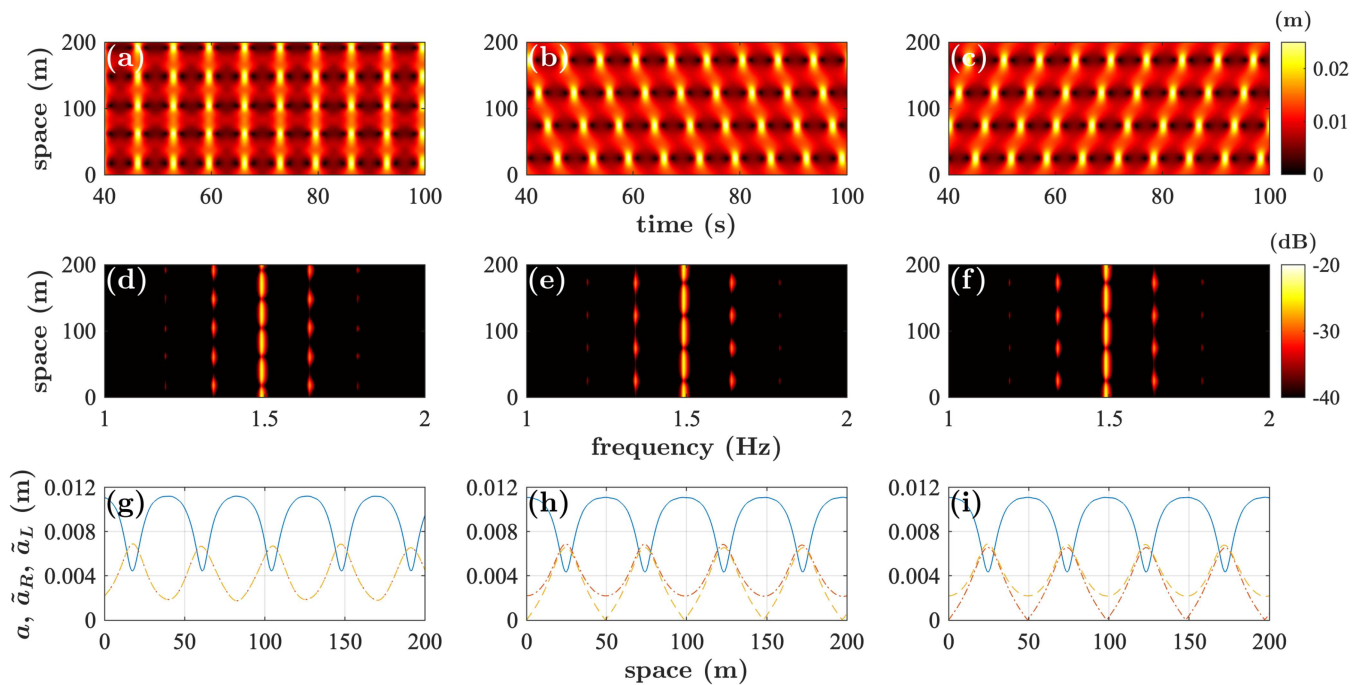
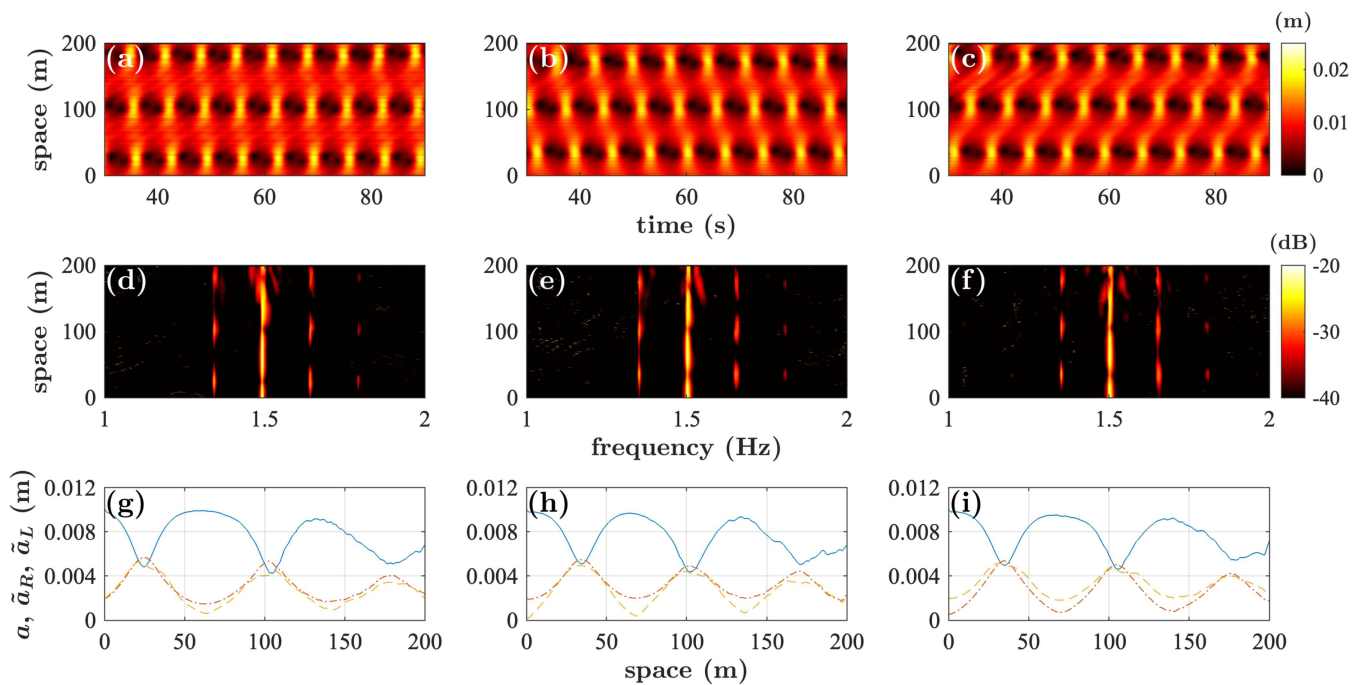


FIG. 5. Evolution of the wave envelopes' maxima as collected from wave tank data (solid blue lines), numerical NLSE simulations (dashed black lines), and ESBI simulations (dashed-dotted red lines) for (a) pure AB evolution, (b) symmetric perturbation of wave train, (c) left sideband perturbation only, and (d) right sideband perturbation only.



**FIG. 6.** Long-running numerical NLSE simulations corresponding to the cases described in Fig. 3. (g)–(i) show the evolution of the carrier (solid blue lines), left sideband (dashed–dotted red lines), and right sideband (dashed yellow lines) amplitudes to the cases above. The spatial recurrence period has been identified to be 45 m, which corresponds to  $65\lambda$ .



**FIG. 7.** Long-running fully nonlinear ESB simulations corresponding to Figs. 3 and 6. (g)–(i) show the evolution of the carrier (solid blue lines), left sideband (dashed–dotted red lines), and right sideband (dashed yellow lines) amplitudes to the cases above. The spatial recurrence period has been identified to be 83 m, which corresponds to  $120\lambda$ .

We now turn our attention to the long-term evolution of the MI process, which implies a recurrent focusing process related to the FPUT recurrence. The latter process has been experimentally studied in hydrodynamics.<sup>13,17,62–64</sup> In this connection, we only study the case of unstable Stokes waves. The NLSE simulation results of the three types of initial perturbations, described in Fig. 3 are depicted in Fig. 6.

In addition to the slight delay in the focusing between the double-sideband and single-sideband excitations, already observed in the experiments, we can also notice a particular shift in the recurrent cycles, which appears to be due to the slight change of the value of group velocity in the asymmetric excitation. We are reminded that all measurements have been aligned by the value of the deep-water group velocity  $c_g = \frac{\omega}{2k}$ . Moreover, there is almost no distinction in the recurrence period between the respective single-left and single-right sideband perturbation cases. The same features are also observed in our fully nonlinear simulations pictured in Fig. 7.

However, we can notice that the first focusing cycle is clearly further lagged compared to the NLSE predictions and so also the recurrent focusing period, which is clearly longer, see Figs. 6(a)–6(c) as well as Figs. 7(a)–7(c). In fact, we conjecture that this is the result of the mean flow contribution, which is not considered in the simplified NLSE framework.<sup>13,58,59,64,65</sup> We would also like to highlight that the same characteristics in the recurrence-shift and trends are also observed for spectrally truncated ABs, but will not be discussed in the paper for brevity. In addition, the minor change in group velocity of the breathing, observed along propagation in the time domain, can be directly related to the varying spectral asymmetry during the nonlinear focusing and four-wave mixing processes, see Figs. 3(b)–3(c). This behavior is fully captured by the NLSE simulations [Figs. 6(b)–6(c)], which confirm previous predictions from Ref. 66 highlighting the impact of initial asymmetric wave condition, namely, a quasi-bichromatic wave formed by the carrier wave perturbed by a single sideband. In the phase plane, the trajectory would also be different from those obtained using the exact AB theory or sinusoidal excitation (i.e., a truncated AB with a symmetric spectrum) shown in Ref. 17. It is also worth to mention that fully nonlinear ESBI simulations [Figs. 7(b)–7(c)] recover and underline such dynamics.

## V. CONCLUSION

Our experimental investigation shows that a hydrodynamic MI process can be triggered either from a one single sideband perturbation only, i.e., from a two-wave system or a spectrally truncated AB through the application of a high- or low-pass frequency filtering from the peak frequency, and at an early stage of wave group compression. The experiments are in good agreement with the fully nonlinear hydrodynamic ESBI-based numerical wave tank simulations. We emphasize that NLSE simulations predict the same experimental wave evolution trends. However, due to the higher accuracy of the ESBI framework with the respect to the order of nonlinearity, we decided not to add these in the paper. Long-running NLSE and ESBI simulations of the perturbation processes show a distinct phase shift in the recurrent cycles during the FPUT focusing recurrence. The numerical ESBI wave tank simulations reveal a distinct delay in the wave focusing compared to the NLSE results for

all cases (symmetric and asymmetric sideband perturbations), which we attribute to the deep-water meanflow contribution, not modeled to third-order in steepness in the classical NLSE. Our work may motivate future experimental studies, which will also incorporate the effects of dissipation and forcing for similar MI-type initializations. Moreover, we believe that asymmetric instability excitations in irregular wave fields require further attention to understand the broad effects of quasi four-wave resonant interactions in nonlinear dispersive media.

## ACKNOWLEDGMENTS

Y.H. acknowledges the support from the Distinguished Postdoctoral Fellowship Scheme of the Hong Kong Polytechnic University (PolyU). Y.H. and J.W. show gratitude to the sponsorship provided by the University Grants Committee, Hong Kong (P0039692), PolyU, Hong Kong (A0048708), Research Institute for Sustainable Urban Development at PolyU, Hong Kong (P0042840), Department of Science and Technology of Guangdong Province, China (22202206050000278). A.C. acknowledges support from Kyoto University's Hakubi Center for Advanced Research.

## AUTHOR DECLARATIONS

### Conflict of Interest

The authors have no conflicts to disclose.

### Author Contributions

**Yuchen He:** Conceptualization (equal); Formal analysis (equal); Investigation (equal); Methodology (equal); Project administration (equal); Resources (equal); Software (equal); Validation (equal); Visualization (equal); Writing – original draft (equal); Writing – review & editing (equal). **Jinghua Wang:** Conceptualization (equal); Formal analysis (equal); Investigation (equal); Methodology (equal); Project administration (equal); Resources (equal); Software (equal); Validation (equal); Visualization (equal); Writing – original draft (equal); Writing – review & editing (equal). **Bertrand Kibler:** Conceptualization (equal); Formal analysis (equal); Investigation (equal); Methodology (equal); Project administration (equal); Resources (equal); Software (equal); Validation (equal); Visualization (equal); Writing – original draft (equal); Writing – review & editing (equal). **Amin Chabchoub:** Conceptualization (equal); Formal analysis (equal); Investigation (equal); Methodology (equal); Project administration (equal); Resources (equal); Software (equal); Validation (equal); Visualization (equal); Writing – original draft (equal); Writing – review & editing (equal).

## DATA AVAILABILITY

The data that support the findings of this study are available from the corresponding authors upon reasonable request.

## REFERENCES

- <sup>1</sup>D. Benney and A. C. Newell, *J. Math. Phys.* **46**, 133 (1967).
- <sup>2</sup>M. Remoissenet, *Waves Called Solitons: Concepts and Experiments* (Springer Science & Business Media, 2013).
- <sup>3</sup>A. R. Osborne, in *Scattering* (Elsevier, 2002), pp. 637–666.



- <sup>4</sup>M. J. Ablowitz, *Nonlinear Dispersive Waves: Asymptotic Analysis and Solitons* (Cambridge University Press, 2011), Vol. 47.
- <sup>5</sup>T. B. Benjamin, *Proc. R. Soc. London, Ser. A* **299**, 59 (1967).
- <sup>6</sup>H. Bailung and Y. Nakamura, *J. Plasma Phys.* **50**, 231 (1993).
- <sup>7</sup>K. Tai, A. Hasegawa, and A. Tomita, *Phys. Rev. Lett.* **56**, 135 (1986).
- <sup>8</sup>P. Everitt, M. Sooriyabandara, M. Guasoni, P. Wigley, C. Wei, G. McDonald, K. Hardman, P. Manju, J. Close, C. Kuhn *et al.*, “*Phys. Rev. A* **96**, 041601 (2017).
- <sup>9</sup>V. E. Zakharov and L. A. Ostrovsky, *Physica D* **238**, 540 (2009).
- <sup>10</sup>H. C. Yuen and B. M. Lake, *Adv. Appl. Mech.* **22**, 67 (1982).
- <sup>11</sup>E. Fermi, P. Pasta, S. Ulam, and M. Tsingou, “Studies of the nonlinear problems,” Technical Report [Los Alamos National Laboratory (LANL), Los Alamos, 1955].
- <sup>12</sup>S. Trillo and S. Wabnitz, *Opt. Lett.* **16**, 986 (1991).
- <sup>13</sup>M. P. Tulin and T. Waseda, *J. Fluid Mech.* **378**, 197 (1999).
- <sup>14</sup>C. M. Chiang, M. Stiassnie, and D. K. Yue, *Theory and Applications of Ocean Surface Waves: Part 1: Linear Aspects Part 2: Nonlinear Aspects* (World Scientific, 2005).
- <sup>15</sup>T. Dauxois, *Phys. Today* **61**(1), 55 (2008).
- <sup>16</sup>A. Babanin, *Breaking and Dissipation of Ocean Surface Waves* (Cambridge University Press, 2011).
- <sup>17</sup>O. Kimmoun, H. Hsu, H. Branger, M. Li, Y. Chen, C. Kharif, M. Onorato, E. J. Kelleher, B. Kibler, N. Akhmediev *et al.*, *Sci. Rep.* **6**, 28516 (2016).
- <sup>18</sup>D. Pierangeli, M. Flammini, L. Zhang, G. Marcucci, A. Agrat, P. Grinevich, P. Santini, C. Conti, and E. DelRe, *Phys. Rev. X* **8**, 041017 (2018).
- <sup>19</sup>A. Mussot, C. Naveau, M. Conforti, A. Kudlinski, F. Copie, P. Szriftgiser, and S. Trillo, *Nat. Photonics* **12**, 303 (2018).
- <sup>20</sup>N. Akhmediev, V. Eleonskii, and N. Kulagin, *Sov. Phys. JETP* **62**, 894 (1985). See [http://www.jetp.ras.ru/cgi-bin/dn/e\\_062\\_05\\_0894.pdf](http://www.jetp.ras.ru/cgi-bin/dn/e_062_05_0894.pdf).
- <sup>21</sup>D. H. Peregrine, *ANZIAM J.* **25**, 16 (1983).
- <sup>22</sup>J. M. Dudley, G. Genty, F. Dias, B. Kibler, and N. Akhmediev, *Opt. Express* **17**, 21497 (2009).
- <sup>23</sup>B. Kibler, J. Fatome, C. Finot, G. Millot, F. Dias, G. Genty, N. Akhmediev, and J. M. Dudley, *Nat. Phys.* **6**, 790 (2010).
- <sup>24</sup>A. Chabchoub, N. Hoffmann, and N. Akhmediev, *Phys. Rev. Lett.* **106**, 204502 (2011).
- <sup>25</sup>H. Bailung, S. Sharma, and Y. Nakamura, *Phys. Rev. Lett.* **107**, 255005 (2011).
- <sup>26</sup>A. Chabchoub, B. Kibler, J. M. Dudley, and N. Akhmediev, *Philos. Trans. R. Soc. A* **372**, 20140005 (2014).
- <sup>27</sup>D. Luo, Y. Jin, J. H. Nguyen, B. A. Malomed, O. V. Marchukov, V. A. Yurovsky, V. Dunjko, M. Olshani, and R. Hulet, *Phys. Rev. Lett.* **125**, 183902 (2020).
- <sup>28</sup>A. Romero-Ros, G. Katsimiga, S. Mistakidis, S. Mossman, G. Biondini, P. Schmelcher, P. Engels, and P. Kevrekidis, *Phys. Rev. Lett.* **132**, 033402 (2024).
- <sup>29</sup>N. Akhmediev and V. Korneev, *Theor. Math. Phys.* **69**, 1089 (1986).
- <sup>30</sup>M. Conforti, A. Mussot, A. Kudlinski, S. Trillo, and N. Akhmediev, *Phys. Rev. A* **101**, 023843 (2020).
- <sup>31</sup>G. Vanderhaegen, C. Naveau, P. Szriftgiser, A. Kudlinski, M. Conforti, A. Mussot, M. Onorato, S. Trillo, A. Chabchoub, and N. Akhmediev, *Proc. Natl. Acad. Sci. U.S.A.* **118**, e2019348118 (2021).
- <sup>32</sup>K. Tai, A. Tomita, J. Jewell, and A. Hasegawa, *Appl. Phys. Lett.* **49**, 236 (1986).
- <sup>33</sup>A. Alberello, E. Părau, and A. Chabchoub, *Sci. Rep.* **13**, 13654 (2023).
- <sup>34</sup>T. B. Benjamin and J. E. Feir, *J. Fluid Mech.* **27**, 417 (1967).
- <sup>35</sup>A. Shabat and V. Zakharov, *Sov. Phys. JETP* **34**, 62 (1972). See [http://www.jetp.ras.ru/cgi-bin/dn/e\\_034\\_01\\_0062.pdf](http://www.jetp.ras.ru/cgi-bin/dn/e_034_01_0062.pdf).
- <sup>36</sup>N. N. Akhmediev and A. Ankiewicz, *Solitons: Nonlinear Pulses and Beams* (Chapman & Hall, 1997).
- <sup>37</sup>K. B. Dysthe and K. Trulsen, *Phys. Scr.* **T82**, 48 (1999).
- <sup>38</sup>B. Wetzel, M. Erkintalo, G. Genty, K. Hammani, B. Kibler, J. Fatome, C. Finot, F. Dias, N. Akhmediev, G. Millot *et al.*, *SPIE Newsroom* **5**, 1 (2011).
- <sup>39</sup>M. Onorato, A. R. Osborne, and M. Serio, *Phys. Rev. Lett.* **96**, 014503 (2006).
- <sup>40</sup>T. Waseda, T. Kinoshita, and H. Tamura, *J. Phys. Oceanogr.* **39**, 621 (2009).
- <sup>41</sup>A. Galchenko, A. V. Babanin, D. Chalikov, I. Young, and T.-W. Hsu, *J. Phys. Oceanogr.* **40**, 2313 (2010).
- <sup>42</sup>C. Kharif and J. Touboul, *Eur. Phys. J. Spec. Top.* **185**, 159 (2010).
- <sup>43</sup>J. N. Steer, A. G. Borthwick, D. Stagonas, E. Buldakov, and T. S. van den Bremer, *J. Fluid Mech.* **884**, A40 (2020).
- <sup>44</sup>J. H. Li, K. S. Chiang, and K. W. Chow, *JOSA B* **28**, 1693 (2011).
- <sup>45</sup>S. Mendes and J. Kasparian, *Phys. Rev. E* **106**, 065101 (2022).
- <sup>46</sup>Y. Li, *J. Fluid Mech.* **960**, A33 (2023).
- <sup>47</sup>D. Andrade and R. Stuhlmeier, *J. Fluid Mech.* **958**, A17 (2023).
- <sup>48</sup>Y. Li and A. Chabchoub, *Geophys. Res. Lett.* **51**, e2023GL107381, <https://doi.org/10.1029/2023GL107381> (2024).
- <sup>49</sup>Y. He, G. Ducroz, N. Hoffmann, J. Dudley, and A. Chabchoub, *Physica D* **439**, 133342 (2022).
- <sup>50</sup>J. Spinneken and C. Swan, *Ocean Eng.* **36**, 539 (2009).
- <sup>51</sup>J. Spinneken and C. Swan, *Ocean Eng.* **36**, 549 (2009).
- <sup>52</sup>J. Yang, *Nonlinear Waves in Integrable and Nonintegrable Systems* (SIAM, 2010).
- <sup>53</sup>Y. He, A. Slunyaev, N. Mori, and A. Chabchoub, *Phys. Rev. Lett.* **129**, 144502 (2022).
- <sup>54</sup>J. Wang, Q. Ma, S. Yan, and B. Liang, *Front. Phys.* **9**, 593394 (2021).
- <sup>55</sup>J. Wang and Q. W. Ma, *Procedia Eng.* **126**, 597 (2015).
- <sup>56</sup>J. Wang, *arXiv:2310.19840* (2023).
- <sup>57</sup>D. Clamond, D. Fructus, J. Grue, and Ø. Kristiansen, *J. Comput. Phys.* **205**, 686 (2005).
- <sup>58</sup>L. Shemer and L. Alperovich, *Phys. Fluids* **25**, 051701 (2013).
- <sup>59</sup>A. Slunyaev, E. Pelinovsky, A. Sergeeva, A. Chabchoub, N. Hoffmann, M. Onorato, and N. Akhmediev, *Phys. Rev. E* **88**, 012909 (2013).
- <sup>60</sup>A. Chabchoub, T. Waseda, M. Klein, S. Trillo, and M. Onorato, *Phys. Rev. Fluids* **5**, 114801 (2020).
- <sup>61</sup>Y. He, A. Witt, S. Trillo, A. Chabchoub, and N. Hoffmann, *Phys. Rev. E* **106**, L043101 (2022).
- <sup>62</sup>S. Trillo, G. Deng, G. Biondini, M. Klein, G. Clauss, A. Chabchoub, and M. Onorato, *Phys. Rev. Lett.* **117**, 144102 (2016).
- <sup>63</sup>O. Kimmoun, H. Hsu, B. Kibler, and A. Chabchoub, *Phys. Rev. E* **96**, 022219 (2017).
- <sup>64</sup>D. Eeltink, A. Armaroli, C. Luneau, H. Branger, M. Brunetti, and J. Kasparian, *Nonlinear Dyn.* **102**, 2385 (2020).
- <sup>65</sup>A. Gmel, C. Montessuit, A. Armaroli, D. Eeltink, A. Chabchoub, J. Kasparian, and M. Brunetti, *Phys. Fluids* **35**, 087128 (2023).
- <sup>66</sup>B. Frisquet, B. Kibler, and G. Millot, *Phys. Rev. X* **3**, 041032 (2013).